JACS
JOURNAL OF THE AMERICAN CHEMICAL SOCIETY

ARTICLE

pubs.acs.org/JACS

Photoswitching-Induced Frequency-Locked Donor−Acceptor Fluorescence Double Modulations Identify the Target Analyte in Complex Environments

Zhiyuan Tian,*[,†] Wuwei Wu,[‡] Wei Wan,[‡] and Alexander D. Q. Li*[,‡]

[†]College of Chemistry and Chemical Engineering, Graduate University of Chinese Academy of Sciences (GUCAS), Beijing, P. R. China 100049

[‡]Department of Chemistry and Center for Materials Research, Washington State University, Pullman, Washington 99164, United States

ABSTRACT: Precisely identifying biological targets and accurately extracting their relatively weak signals from complicated physiological environments represent daunting challenges in biological detection and biomedical diagnosis. Fluorescence techniques have become the method of choice and offer minimally invasive and ultrasensitive detections, thus, providing a wealth of information regarding the biological mechanisms in living systems. Despite fluorescence analysis has advanced remarkably, conventional detections still encounter considerable limitations. This stems from the fact that the fluorescence intensity signal (I) is sensitive and liable to numerous external factors including temperature, light source, medium characteristics, and dye concentration. The interferences exasperatingly undermine the precision of measurements, and frequently render the signal undetectable. For example, fluorescence from single-molecule emitters can be measured on glass substrates under optimum conditions, but single-molecule events in complicated physiological environments such as live cells can hardly be detected because of autofluorescence interference and other factors. Furthermore, traditional intensity (I) and wavelength (λ) measurements do not reveal the interactive nature between the donor and the acceptor. Thus, innovative detection strategies to circumvent these aforementioned limitations of the conventional techniques are critically needed. With the use of photoswitching-induced donor−acceptor-fluorescence double modulations, we present a novel strategy that introduces three additional physical parameters: modulation amplitude (A), phase shift ($\Delta\Phi$), and lock-in frequency (ω), and demonstrate that such a strategy can circumvent the limitation of the conventional fluorescence detection techniques. Together, these five physical quantities (I, λ, A, $\Delta\Phi$, ω) reveal insightful information regarding molecular interactive strength between the probe and the analyte and enable extracting weak-fluorescence spectra from large interfering noises in complex environments.

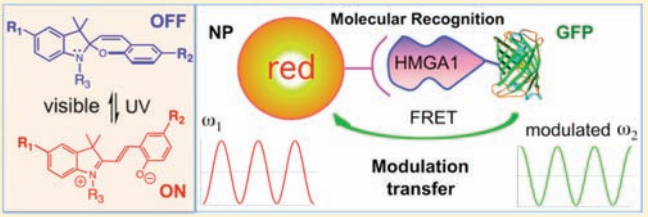

INTRODUCTION

Fluorescence-based detection has played active roles at the forefront of bioanalysis because it enables ultrahigh sensitivity, produces excellent spatiotemporal resolution, and can be easily manipulated.[1−5] Conventional techniques typically measure fluorescence intensity versus wavelength ($I \sim \lambda$), and are thus unable to resolve weak signals from strong noises in the same frequency region such as interfering fluorescence or cell autofluorescence.[6−8] Moreover, the interactive nature of a fluorescent donor−acceptor pair cannot be probed using the intensity spectra alone. Despite recent efforts using nanoprobes to detect biological targets such as proteins,[9,10] the dynamic interactions of probes with living systems are still poorly understood and effective detection strategies are highly desirable.[11−13] Currently, fluorescence resonance energy transfer (FRET) has been proven to be a very powerful technique to study the dynamic interactions in live cells.[14,15] Adding frequency-dependent information to FRET will not only link one molecular motion to another at the nanoscale, but also further reveal the insightful mutual characteristics between the interacting partners at any time.

The tremendous utility of FRET resides at the moment when fluorescent acceptor signal rises and simultaneously the donor signal falls. The opposite swing of the donor and acceptor fluorescence establishes the intrinsic correlation, confirming molecular interactions have occurred. On the basis of such a unique validation, FRET imaging microscope has been applied to detect protein−protein interactions and protein conformation changes *in vivo*[14,15] or to explore the information on the immediate nanoenvironment.[16−18] FRET, however, is good at measuring the moment when FRET occurs, but cannot provide such correlating information about the interactive process as time elapses. Over biological time scales of hours and days, a single pair of FRET cannot provide reliable information over time. Had FRET occurred at a controlled frequency, one could match donor and acceptor frequency and validate the existence of energy transfer, molecular interactions, at any time.

Modulating the excitation-source intensity induces fluorescence modulation.[19,20] At low modulation frequency (500−5000 Hz), the emission closely follows the excitation. Hence, the phase shift is near zero and demodulation ratio is close to one. As the modulation frequency increases to ∼10 MHz, the finite lifetime

Received: June 3, 2011
Published: August 24, 2011

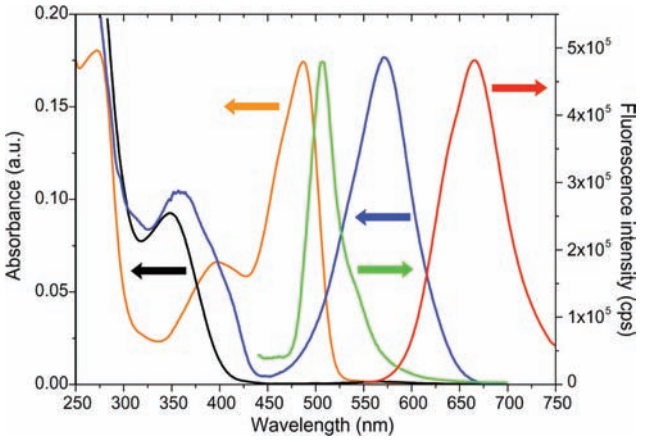

Figure 1. UV−visible absorption spectra of spiropyran (black), merocyanine (blue), and GFP (orange) are compared and contrasted to fluorescence emission spectra of GFP (green) and merocyanine (red).

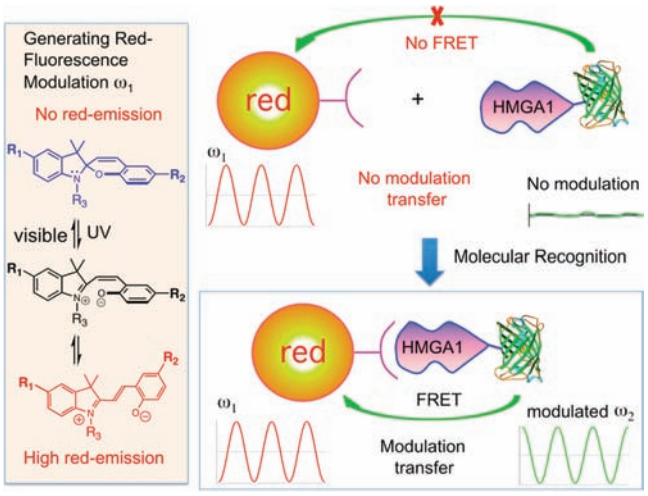

Figure 2. Schematic representation demonstrating photoswitching-induced fluorescence modulation of spiropyran-containing nanoparticles (red-fluorescence modulation) and the lock-in fluorescence-modulation-transfer from nanoparticles to green fluorescent proteins (green-fluorescence modulation) based on modulating fluorescence resonance energy transfer efficiency.

of the chromophore formation limits the emission from precisely following the excitation. As a result, fluorescence phase drifts away from the excitation phase and the modulated emission amplitude decreases. The frequency-dependent phase shift and amplitude alteration contain lifetime information; fluorescence lifetime can be determined by fitting phase shift or amplitude ratio as functions of modulation frequency. Such frequency-domain lifetime measurements demonstrate the power of modulation. However, modulating excitation intensity also imparts modulation in fluorescent interferences and thereby signals and noises cannot be separated because both contain identical frequency information. In a FRET pair, modulating the excitation intensity of the donor will not change the FRET efficiency and thus offer no new information.

However, a photoswitchable fluorescent acceptor can induce both fluorescence modulation and FRET efficiency undulation without modulating the excitation intensity. Photoswitching in photochromic component triggered by controlled light pulses virtually varies the population of fluorescent acceptor within a nanoprobe. Such a light-driven population change of the fluorescent acceptors in turn modulates the nearby fluorescent donors to oscillate in a locked frequency via FRET. When the analyte (fluorescent donor) exclusively binds to the photoswitchable nanoprobe (fluorescent acceptor), fluorescence modulation of the nanoprobe only transfers to the bound donor because FRET is highly localized within nanometer vicinity. Consequently, interfering noises receive no modulation. Therefore, signals from bound FRET pairs can be effectively separated from interfering noises. In other words, controlled light-pulse sequences induce the correlated synchronized oscillation between the donor and the acceptor, thus, separating the information-rich signals from nonoscillating (zero-frequency) noises. In addition, different analytes linked to fluorescent donors distinctively interact with the photoswitchable fluorescent acceptor, thus, generating characteristic parameters (A, $\Delta\Phi$, and ω) for further identification.

In this paper, we report that photoswitching-induced double fluorescence modulations reveal interactive nature between the fluorescent donor and the photoswitchable acceptor. The linchpin of this innovative technology is the photoswitchable fluorescent probes,[21−24] whose revolutionary role in wide-field super-resolution fluorescence imaging has already been demonstrated, because they reversibly interconvert between two distinct states.[25−30] Such improved detection strategy outperforms conventional techniques, yielding enhanced precision and results independent of external factors such as low analyte concentrations. Finally, such a frequency-locked modulation enables deciphering weak modulated signals from strong nonmodulated noises, and determines dissociation constant (K_d) of the binding complexes using the phase shift information.

RESULTS AND DISCUSSION

Previously synthesized polymer nanoparticles (NP), typically 61-nm in diameter, contain photoswitchable red fluorescent acceptors as the photostimuli responsive units. Such particles are synthesized using a water-soluble carboxylate initiator to generate negatively charged surfaces.[12,13,31] Obviously, negatively charged nanoparticles interact with positively charged proteins, whose interactive nature can be effectively probed using fluorescence double modulations. The photoswitchable dyes are based on spiropyran−merocyanine derivatives. Spiropyran molecules undergo reversible ring-opening to yield merocyanine upon UV irradiation. Specifically, as shown in Figure 1, merocyanine absorbs intensely in the region of 450−650 nm with maximum at 570 nm, which overlaps well with the fluorescence bands of fluorescein dyes and green fluorescent protein (GFP), thus, enabling FRET. In other words, merocyanine will effectively quench the green fluorescence of GFP or fluorescein dye. In contrast, spiropyran does not absorb in the visible region because its first absorption maximum occurs at 350 nm (Figure 1). Thus, spiropyran is unable to function as the energy acceptor to quench the fluorescence of either GFP at 508 nm or fluorescein at 512 nm because of energetic uphill. Moreover, merocyanine as an energy acceptor strongly fluoresces red emission, λ_{max} = 665 nm, which has little fluorescence signal crosstalk with the green fluorescence of GFP.

Consequently, converting such a key photochromophore from spiropyran to merocyanine photochemically not only turns on its own red-fluorescence but also activates a fluorescent acceptor that enables energy transfer from GFP to merocyanine.

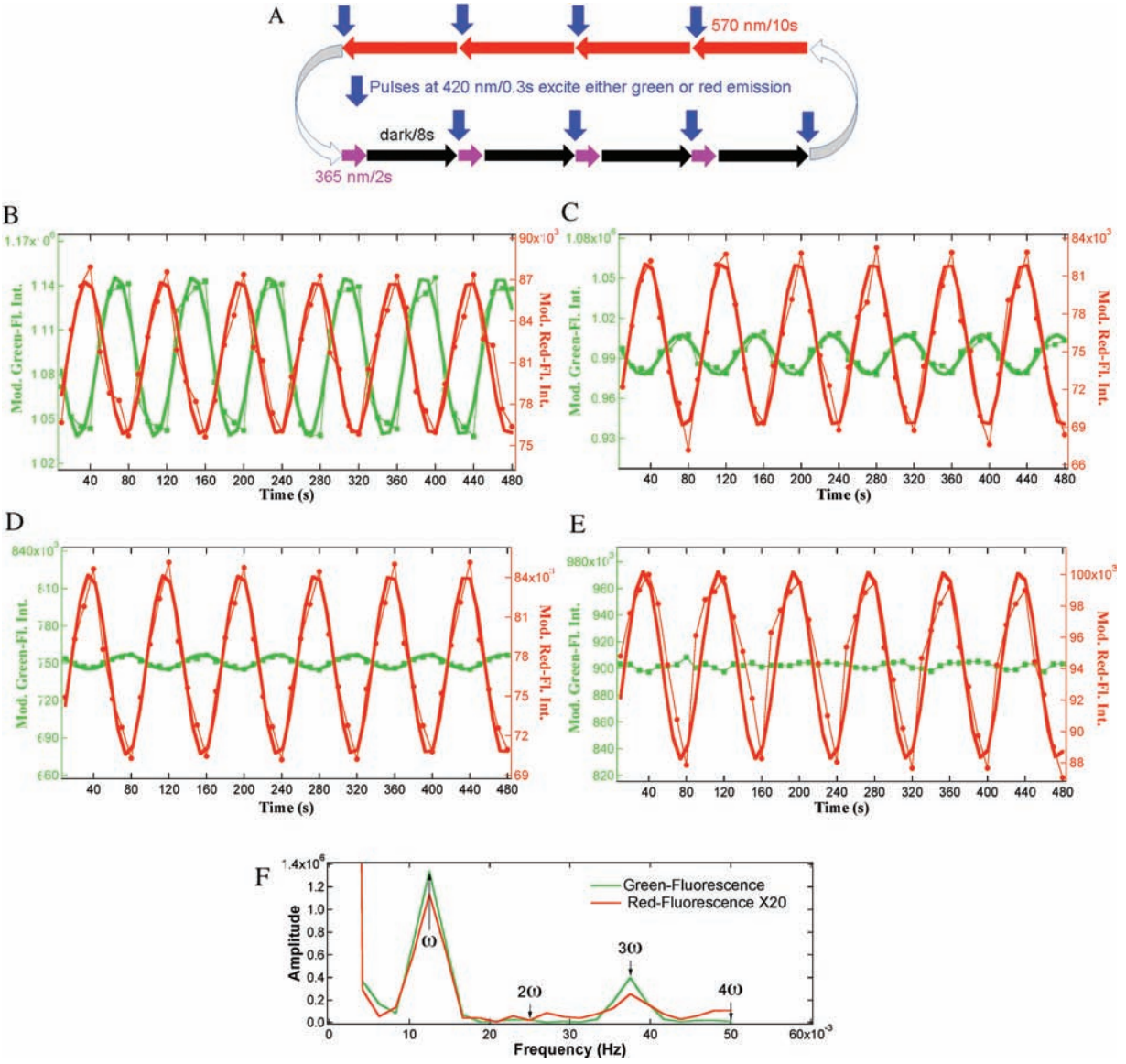

Figure 3. Photoswitching-and-FRET based donor−acceptor fluorescence double modulations. (A) Programmed pulse sequences that elicited nanoparticles photoswitching. Photoswitching pulses in (A) induce the correlated synchronized oscillation between the acceptor (nanoparticle) and the donor: HMGA1-GFP (B), GFP (C), HMGA1-fluorescin (D), and free fluorescein (E), respectively. When the green fluorescent analytes interact with and bind to the nanoparticles, the acceptor-fluorescence modulation is transferred to the green fluorescent donor at the same locked frequency (ω). (F) Fourier transformation (FT) on data shown in (B) reveals that modulated red- and green-fluorescence signals contains odd terms only (ω, 3ω, etc.).

The FRET efficiency based on the fluorescent donor is varying because the relative concentrations of the merocyanine and spiropyran are changing. As the ratio of merocyanine-to-spiropyran increases, FRET efficiency increases accompanying red-fluorescence augmentation and green-fluorescence reduction. Switching the triggering pulses from UV to visible light causes the merocyanine-to-spiropyran ratio to diminish, thus, reversing the trend of red- and green-fluorescence. As a result, periodically switching the merocyanine-to-spiropyran ratio in the nanoparticles either strengthens or weakens the FRET efficiency, thus, modulating both the red-fluorescence of the nanoparticles and the green-fluorescence of GFP at a specific and identical frequency.[32] Therefore, interactions or binding between the donor and acceptor create frequency-locked double modulations (Figure 2).

To validate the modulation-transfer concept, we used the photoswitchable nanoparticle to modulate the fluorescence signals of four representative samples serving as the energy donors. For general analyses, the configuration that two antibodies sandwich the analyte (similar to Figure 2) provides the most versatile approach to frequency double modulations: one will be conjugated to the green fluorophore and the other to the photoswitchable nanoparticle. To simplify unnecessary labeling in this report, we use the interactions between the nanoparticles and proteins to demonstrate the FRET modulation. The first sample was the high mobility group A (HMGA1) protein fused with green fluorescent protein (GFP): GFP-HMGA1. The second sample was GFP alone. The third sample was HMGA1 protein labeled with ~4 fluorescein dyes and the fourth sample was simply fluorescein. Programmed switching and probing light

pulses shown in Figure 3A induce red- and green-fluorescence double modulations as displayed in Figure 3B−E. Specifically, four 365-nm UV pulses at 2-s duration were employed to drive the forward switching from spiropyran to merocyanine within the nanoparticles. In the forward switching half-periods, fluorescence was measured using 420-nm excitation with 0.3-s duration after an 8-s delay from the UV pulses. The backward switching, from merocyanine to spiropyran, was fulfilled using four 10-s visible pulses at the merocyanine absorption band, 570 nm, and fluorescence was measured using 420-nm illumination for 0.3-s duration immediately after the switching pulse without delay. The reason that 420-nm light was used to excite fluorescence was that there is no net switching between spiropyran and merocyanine at 420 nm. At this wavelength, fluorescence excitation can be carried out independently without imparting net switching of the dyes.

The designed pulse sequence in Figure 3A photochemically isomerizes dyes between two distinct states: the nonfluorescent spiropyran and the red-fluorescent merocyanine. The periodic oscillation between spiropyran and merocyanine induces red-fluorescence from nanoparticles to oscillate at ω_{red} = 12.5 mHz frequency. This oscillation further transfers modulating frequency to the fluorescent donor GFP, which emits green-fluorescence at the same oscillating frequency ω_{green} =12.5 mHz. Such intrinsic transfer of locked modulation frequency ($\omega_{red} = \omega_{green}$) was observed for all interacting partners. The negatively charged fluorescein does not attract to negatively charged nanoparticles, and thus, modulating red-fluorescence at 12.5 mHz induced no green-fluorescence oscillation in fluorescein (Figure 3E). Therefore, only interacting pairs propagated fluorescence modulation.

Fourier transformation (FT) was applied to the experimentally modulated red- and green-fluorescence signals plotted in Figure 3B. The FT results indicate that the fluorescence oscillation contains only the odd order terms such as ω, 3ω, 5ω, and so forth. Even order contributions (2ω, 4ω, 6ω, etc.) are absent (Figure 3F). On the basis of these facts, theoretical fitting to the experimentally modulated fluorescence intensity uses only odd terms as indicated in eq 1.

$$I = I_0 + A_1 \sin(\omega t + \Phi_1) + A_3 \sin(3\omega t + \Phi_3) + A_5 \sin(5\omega t + \Phi_5) + A_7 \sin(7\omega t + \Phi_7) \quad (1)$$

where I represents red- or green-fluorescence intensity; I_0 is the DC components of fluorescence intensity; and A_1, A_3, A_5, A_7 are modulation amplitude at the fundamental frequency (ω), third harmonic frequency (3ω), fifth harmonic frequency (5ω), and seventh harmonic frequency (7ω); Φ_1, Φ_3, Φ_5, and Φ_7 represent the phases related to different harmonic contributions. The nonlinear curve fittings yield R^2 values from 0.90 to 0.95, validating intrinsic frequency locking relationship revealed by FT.

What is interesting is that the red-fluorescence and green-fluorescence are not oscillating perfectly out of phase (180°), but rather phase shift by $\Delta\Phi$ = 140 ± 4° for GFP-HMGA1-NP samples. The modulated magnitude transfer is very strong: an input red-fluorescence modulation at A_1^{red} = 11 kcps generates an output green-fluorescence modulation of A_1^{green} = 110 kcps, indicating strong binding. This generates a ratio of modulation amplitude, A_1^{green}/A_1^{red} = 10.0 because the FRET efficiency is high. For GFP-NP samples, the modulation amplitude dropped (A_1^{green}/A_1^{red} = 2.3) and a different phase shift ($\Delta\Phi = 157 \pm 3°$) was observed. Moreover, Fluorescein dye labeled HMGA1 protein interacts weakly with the nanoparticle when compared to the GFP-HMGA1 fusion protein because bioconjugation with fluorescein dyes have converted some positively charged lysine residues to nonbinding amide groups. The phase shift changed to 177 ± 3°, near the exact opposite phase and the modulation ratio faded to only A_1^{green}/A_1^{red} = 0.9, indicating that nanoparticles bind the dye-labeled HMGA1 weakly. Finally, free negatively charged fluorescein dye does not interact with the negatively charged nanoparticles. An input of 12.5-mHz red-fluorescence frequency and a large A_1^{red} = 12 kcps magnitude modulation, even larger than the input for the case of GFP-HMGA1-NP, induced no oscillation in the fluorescein green-fluorescence, $A_1^{green}/A_1^{red} \approx 0$ because K_d is very large. These data revealed that the phase shifts and magnitude modulation effectively gauged the interactive nature (K_d) between the red-emitting NPs and green-emitting analytes. As the binding strength decreased and the interactions faded, the modulation transfer abated and phase difference approached the exact opposite antiphase.

The fading of the modulation amplitude transfer is understandable, but phase-shift changes are nontrivial. A single fluorescent donor−acceptor pair should always oscillate in antiphase synchronization, or a phase shift of 180°. The phase-shift facts suggest that the merocyanine in the NP functions as two fluorescent acceptors but one emitter. Specifically, a nonfluorescent transient intermediate (*cis*-merocyanine like) is expected to involve in the interconversion process between the nonfluorescent ring-closed spiropyran and the fluorescent ring-opened merocyanine (*trans*-merocyanine).[33−35] Molecular modeling work carried out by Erwin and co-workers has confirmed that the thermally induced ring-closure is facilitated from the *cis*-merocyanine as opposed to from the *trans*-merocyanine.[36] Resembling spiropyran in structure, the immediately ring-ruptured merocyanine (*cis*-merocyanine) is proposed as the dark merocyanine, an energy acceptor but not an emitter. The equilibrated planar merocyanine (*trans*-merocyanine) functions both as an energy acceptor and an emitter. Experimental data corroborate that the dark twisted merocyanine must have a shorter Förster radius than the bright planar merocyanine. This model explains that the green-fluorescence oscillation changes before red-fluorescence. Furthermore, the bright merocyanine dominantly influences the weakly interacting analytes, shifting the phase difference to near anti-phase synchronization. Unlike a donor−acceptor pair, many photoswitches distributing uniformly within the NP create an interesting situation, where the phase shift is very sensitive to the association and dissociation of the donor−acceptor complexes. Stronger association (low K_d values) leads to faster FRET responses, both radiatively and nonradiatively from the donor and hence advances its phase forward.

Further studies reveal that, although the amplitude ratio is related to binding affinity (K_d), it also scales with concentration: the smaller the K_d values, the larger the amplitude ratio, or alternatively, the higher the concentration, the larger the amplitude ratio. An NP-analyte complex has a fixed K_d constant, and therefore, the amplitude ratio measures the analyte concentration quite accurately (Figure 4A, red). At low concentration, the relationship is linear from 0.2 to 1.2 μM and a saturation behavior is observed beyond 1.6 μM like in most fluorescence detection. However, the phase shift of a given NP-analyte complex does not change as the analyte concentration is varied (Figure 4A, blue). The former behaves like an extensive property while the latter like an intensive one. As a scale invariant parameter, phase-shift divulges the intrinsic characteristics governing the interactions between the analyte and NP. It appears that each phase shift reveals a unique dissociation constant K_d; plotting the

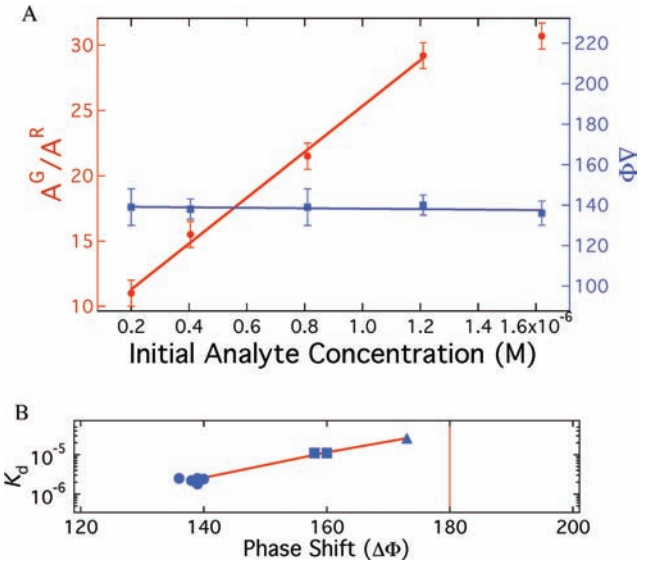

Figure 4. The dependence of the fluorescence modulation amplitude ratio and the independence of phase shift on the analyte concentration; the correlation between the dissociation constant and the phase shift. (A) The amplitude ratio reports the analyte concentration, whereas phase shift does not change with concentration. (B) Further studies reveal that phase shift is proposed to be intrinsically linked to the dissociation constant, K_d. Data from different concentrations cluster together in the $K_d-\Delta\Phi$ map: HMGA-GFP, circles; GFP, squares; HMGA-fluorescein, triangles. Strong interactions shift away from 180° anti-phase in these studies.

dissociation constant K_d against phase shift creates a $K_d\sim\Delta\Phi$ map (Figure 4B), which allows us to deduce K_d values instantly in the modulation experiments. Because fluorescence double modulations generate the amplitude ratio and phase shift simultaneously, both the analyte's concentration and its dissociation constant can be determined simultaneously. Previously, a secondary laser-driven fluorescence modulation was reported;[37] this technique modulates the second laser excitation power to impart fluorescence modulation, similar to most conventional FT techniques and fluorescence modulation for lifetime measurements. This approach is fundamentally different from our work because the modulation originates from the excitation source in the former, whereas fluorescence modulation in the latter originates from the sample due to molecular photoswitching. Also recently, optical lock-in detection (OLID) for selective fluorescence signal recovery emerged. OLID using spiropyran (SP)—merocyanine (MC) dyes was first proposed in 2006[38] and reported a couple of years later.[39,40] Nonetheless, phase-shift based fluorescence detection remains unique. A detection of analyte binding could be positive or negative, but the statistical confidence for positive analyte binding is greatly augmented when the analyte binds with the expected K_d value. This dramatically improves selectivity in fluorescence-based detection assays.

Photoswitching of the sample molecules generates periodic fluorescence oscillation; such acceptor fluorescence oscillation will in turn induce fluorescent donors within the Förster proximity to undulate in a locked frequency. Because only bound analytes are within the Förster proximity and interfering fluorophores are randomly distributed and typically outside the Förster proximity, fluorescence noises will not oscillate with the signal. Therefore, a signal can be technically "extracted" from strong interfering noises using methods similar to the lock-in technology. To experimentally verify such fluorescence signal extraction hypothesis, we selected an extremely challenging interfering fluorophore—fluorescein for the target HMGA1-GFP analyte. Fluorescein not only has a high quantum yield, but also displays similar fluorescence emission peak shape and maximum (λ_{max}= 512 nm) as those of GFP (λ_{max}= 508 nm). Specifically, fluorescein concentration was purposely controlled so that the noise intensity is twice as strong as the GFP fluorescence signal. In such a case, the fluorescence signal of GFP was completely obscured by the interference (Figure 5A). Although stronger in intensity, the green-fluorescence of fluorescein does not respond to the red-fluorescence oscillation of the NP. The weaker GFP green-fluorescence, however, does oscillate with the red-fluorescence through FRET at a locked frequency, ω. Separating the measured fluorescence intensity associated with frequency ω from the zero-frequency components, we successfully extracted the GFP spectra from fluorescein, which has much higher intensity and whose spectrum closely resembles that of pure GFP. After several complete modulation cycles, the modulation frequency, which serves as the intelligent information in the data separation, enables removal of the background noises and interferences. As a result, the "unpolluted" signal of the target analyte was unveiled. Figure 5B demonstrates the "extracted" spectrum has peak shape and position in perfect accordance with that of pure GFP. These results prove that relatively weak signal can be effectively extracted from strong noises using such FRET-based, photoswitching-generated double fluorescence modulations at a locked frequency.

Previously, we demonstrated, both experimentally and theoretically, that periodically oscillating signals can be amplified in frequency-domain imaging.[41] Even though current modulation frequency is low (~mHz), development of advanced instrumentation and faster photoswitchable probes will shorten modulation time well below seconds (>1 Hz), thus allowing to monitor motions in live cells.[41] By integrating the conventional FRET strategy into such a lock-in technology, we successfully detect the signal at a signal-to-noise (S/N) ratio of 0.5, a range normal techniques cannot detect, as demonstrated in Figure 5. Under current experimental conditions, we have successfully extracted the signal from noises even if the S/N ratio is 0.1. Therefore, the present work provides a general approach rather than a specific technique to detect signals with S/N ratios at which we cannot measure using existing techniques. The net result is that frequency modulation detection can be integrated into any existing techniques that detect analytes via measuring fluorescence intensity. Existing fluorescence techniques require a signal-to-noise ratio >1 to calibrate their detection sensitivity. For example, standard FRET assays have a sensitivity of 10 nM at S/N ratio of 3.0 while measuring the fluorescence intensity with no frequency.[42] Adding a modulation frequency as demonstrated in the current work, the S/N ratio can be dropped to S/N = 0.1, that is, a factor of 30 times improvement, at which we can successfully extract signals from noise. This improves the S/N ratio from 0.1 without modulation to 5—10 after frequency lock-in extraction. Thus, when the standard FRET assays are integrated with frequency-modulation method, the expected sensitivity reduces to ~0.3 nM. In fact, detecting low-copy-number targets in the presence of large noises or interferences remains the ultimate challenge. Specifically, our strategy adds a frequency component to the signal, but not noises, and therefore allows noises to be filtered off during frequency-lock-in measurements. As a result, the background fluorescence is essentially removed and the sensitivity increases as more modulation cycles are acquired. Additionally, it

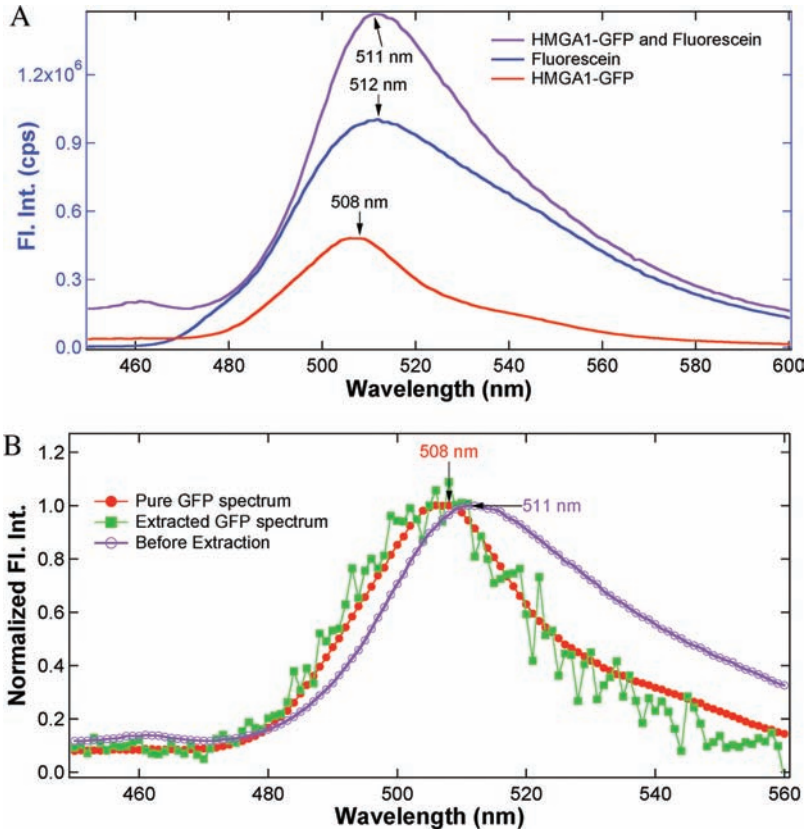

Figure 5. Extracting weak fluorescence signals of the target analyte from strong interfering noises through a fluorescence double-modulation process. (A) Fluorescence spectra of HMGA1-GFP (red), fluorescein (blue), and their mixture (purple) at a 1:2 fluorescence ratio. (B) Because the maximum of fluorescein noise emits at nearly identical region (512 nm) and is twice stronger than the intensity of GFP signal at 508 nm, it completely masks the GFP signal. Photoswitching-induced double modulations cause the GFP signal to oscillate, but not the fluorescein noise, thus, successfully separating the GFP emission spectrum (green squares) form the large noises (purple open circles).

is well-known that sensitivity is proportional to the highly specific binding interactions, such as antigen−antibody interactions.[43,44] Because these optimized binding interactions have already achieved in current biological systems, little room remains for dramatically improving the detection sensitivity via increasing the binding strength. However, intelligently separating the signal from noises fundamentally enables an innovative solution to improve the detection sensitivity of the existing fluorescence assays.

In conclusion, we have demonstrated that adding frequency information to FRET efficiency effectively establishes donor−acceptor fluorescence double modulations. Such FRET-efficiency modulation brings out insightful information, such as the modulation amplitude transfer (A^{green}/A^{red}), phase shift ($\Delta\Phi$), and frequency-locking spectra extraction. The modulation amplitude transfer is related to the bound analyte concentration; the phase shift seems to reveal binding affinity (K_d); the locking frequency reports whether interactions occur at all. Collecting just several modulation cycles improves detection sensitivity by an order of magnitude. Thus, frequency-modulated signals can be easily separated from noises even if the noises are 10 times larger. Such a technology, which can determine specific binding unequivocally, will have significant impact to future fluorescence detections.

MATERIALS AND METHODS

Synthesis of Photochromic Spiropyran (SP) Functionalized with Polymerizable Group. To 100-mL acetonitrile, 3.2 g (20 mmol) of 2, 3, 3-trimethyl-3*H*-indole and 3.0 g (20 mmol) of sodium iodide (NaI) were added. The mixture was then heated to reflux. Subsequently, 3.4 g (22 mmol) of vinylbenzyl chloride was added dropwise and the mixture was further refluxed with stirring for 24 h. After the reaction was cooled to room temperature, the mixture was filtered. The filtrate was distilled under reduced pressure and the residue was dissolved in small amount of chloroform. To the chloroform solution, 30-mL of ether was added. The mixture was sonicated for 10 min and the resulting solid was filtered to yield 7.8 g of 2,3,3-trimethyl-1-(4-vinylbenzyl)-3*H*-indolium iodide in 97% yield as red solid.

To a gently refluxing solution of 0.44 g (2.65 mmol) of 2-hydroxy-5-nitrobenzaldehyde in 30-mL of ethanol, a solution of 1.2 g (2.77 mmol) of 2,3,3-trimethyl-1-(4-vinylbenzyl)-3*H*-indolium iodide and 0.60 mL (4.2 mmol) of triethylamine (Et_3N) in 20-mL of ethanol was added dropwise. The mixture was then refluxed with stirring for 5 h. The filtrate was distilled under reduced pressure. The residue of the distillation was purified using silica column chromatography, which afforded the title compound, SP (830 mg, 74%) as a pale pink solid. MALDI-TOF MS: m/z = 425 $[M + H]^+$; ^1H NMR (300 MHz, CDCl3) δ = 1.30(3H, s), 1.34 (3H, s), 4.20 (1H, d, 17 Hz), 4.50 (1H, d, 17 Hz), 5.20 (1H, d, 10 Hz), 5.71 (1H, d, 17 Hz), 5.91 (1H, d, 10 Hz), 6.35 (1H, d, 8 Hz), 6.66 (1H, dd, 2 and 3 Hz), 6.72 (1H, m), 6.85−6.91 (2H, m), 7.04−7.14 (2H, m), 7.22−7.26 (2H, m), 7.33−7.35 (2H, m), 8.00−8.05 (2H, m).

Synthesis of SP-Containing Polymer Nanoparticles. SP-containing polymer nanoparticles were synthesized via a radical-initiated microemulsion polymerization with minor modifications.[30,31] In a typical polymerization, 30 g of DI water, 0.56 mmol acrylamide (A), and 0.2 mmol acrylic acid (AA) were loaded into a 100-mL flask

equipped with a magnetic stir bar. Bubbling Ar for 30 min to the solution purged oxygen from the system. Next, 0.1 g of Tween 20 surfactant was added. The reaction flask was then immersed into 90 °C oil bath for 5 min followed by an injection of 0.02 mmol 4, 4′-azobis (4-cyanovaleric acid) (ABVA) as the polymerization initiator. After another 5 min, co-monomer mixture containing 3 mg of SP, 0.25 mmol styrene (ST), 0.75 mmol butyl acrylate (BA), and 0.15 mmol divinylbenzene (DVB) was syringe-injected while maintaining the reaction temperature and the stirring speed. Polymerization proceeded for another 3.5 h. The as-prepared polymer nanoparticles were washed with chloroform to remove the unreacted organic reactants. The residual chloroform was then removed from the water phase under reduce pressure, yielding a milky colloid sample.

Characterization of SP-Containing Polymer Nanoparticles. Shape and diameter of the nanoparticle samples were evaluated using a Beckman-Coulter N4 dynamic light scattering (DLS) instrument at fixed scattering angles of 62.6° and 90° using the He−Ne laser 632.8-nm line as the light source. Standard polystyrene microspheres were used to calibrate the instrument before data acquisition. The average particle sizes and size distributions were obtained from the autocorrelation decay functions by CONTIN analysis using standard software package supplied by Beckman-Coulter. The average hydrodynamic diameter of the as-prepared SP nanoparticles obtained from the DLS characterization was 61-nm with a polydispersity index (PDI) less than 10%. A JEOL 1010 transmission electron microscope (TEM) operated at 100 kV was also employed to obtain TEM images of the nanoparticles. The microscope sample was prepared by placing a drop of the polymer dispersion on a carbon-coated Cu grid, followed by solvent evaporation at room temperature. TEM measurements of the as-prepared nanoparticles revealed a narrow size distribution and a relatively smaller average diameter, ∼45 nm, when compared to the hydrodynamic diameter obtained from DLS.

Preparation of the Green-Emitting Fluorophores: GFP, GFP-HMGA1 Fusion Protein, And Fluorescein Labeled HMGA1. High mobility group AT-hook1 (HMGA1) gene was fused with the enhanced green fluorescent protein (EGFP) gene using overlapping polymerase chain reactions (PCR), and cloned into pET24b vector. Plasmids containing GFP or GFP-HMGA1a fusion gene, respectively, were transformed into *Escherichia coli* strain BL21 and their corresponding proteins were produced after using 1 mM IPTG to induce the transfected *E. coli* for 3 h. The His-select Nickel affinity gel (Sigma, Saint Louis, MO) was used to purify GFP or GFP-HMGA1 fuse protein, whose concentrations were determined by measuring solution optical density at 280-nm (OD280). Extinction coefficients of both GFP and HMGA1-GFP proteins were 1.82 mL/(mg·cm). SDS−PAGE indicated the final fusion protein purity was >80%. To make fluorescein-labeled HMGA1 protein, 1 mg of HMGA1 protein was dissolved in 0.5 mL of PBS buffer (pH = 8.0). Next, 0.5 mL of 1 mM fluorescein succinimidyl ester (dissolved in 100 mM bicarbonate, pH = 8.3) was added. The mixture was vortexed and incubated at room temperature for 1 h with constant shaking. Afterward, 0.5 mL of 1 M tris buffer (pH = 8.0) was added to stop the reaction, and the labeled HMGA1 protein was dialyzed against PBS buffer (pH = 8.0) overnight and stored at 4 °C before usage.

Evaluating Phase Shift Using Donor−Acceptor Fluorescence Double Modulations. Photoswitching-induced frequency-locked donor−acceptor fluorescence modulation was carried out employing the pulse sequences presented in the main text (Figure 3). The forward switching, from spiropyran to merocyanine, used four 365-nm UV pulses (purple) at 2-s duration; each pulse was followed by 8-s delay (black) before fluorescence was measured using 420 nm at 0.3-s duration. The backward switching, from merocyanine to spiropyran, used four wide 10-s pulses (red) at the mero-absorption band 570 nm while 420-nm-excited fluorescence was measured immediately, right after each switching pulse. For the three donor−acceptor combinations, whose fluorescence modulation results are presented in the main text and Figure 3, the concentration of the donor, that is, GFP-HMGA1, GFP, and fluorescein-HMGA1, was set at 200 nM while the concentration of the spiropyran-containing nanoparticle was 40 nM. For the combination of fluorescein-nanoparticles, the concentration of fluorescein was 250 nM; nanoparticles, 50 nM. Obviously, even with increased concentration, fluorescence modulation was not transferred from nanoparticles to fluorescein dye, revealing the lack of mutual attraction between fluorescein molecules and nanoparticles. To obtain the modulation curves, nonlinear least-squares fitting using periodic sine functions was performed. The first term, oscillating at the fundamental frequency, dominates the fitting. Therefore, the phase shift for each donor−acceptor pair was determined using the phase difference between the red-fluorescence and the green-fluorescence in the first term.

Extracting Weak Fluorescence Spectrum of HMGA1-GFP from Strong Fluorescein Background. To experimentally verify the fluorescence signal extraction hypothesis, we selected an extremely challenging interfering fluorophore-fluorescein for the targeted HMGA1-GFP analyte. Fluorescein not only has a high quantum yield, but also displays similar fluorescence emission peak shape and maximum (λ_{max}= 512 nm). Both HMGA1-GFP and fluorescein was dissolved in a PBS (pH = 8.0) buffer to simulate a high-background environment. The concentration of fluorescein dye was 300 nM; HMGA1-GFP, 100 nM. With such a concentration ratio, the fluorescence intensity of fluorescein, that is, the simulated background noise, was twice stronger than the fluorescence signal of HMGA1-GFP upon 420-nm excitation. In such a case, the fluorescence signal of GFP was completely obscured by the background, as shown in Figure 5A.

To enable double fluorescence modulations, spiropyran-containing polymer nanoparticles were added to the HMGA1-GFP and fluorescein solution at room temperature. The samples were allowed to equilibrate for 20 min. Such mixed sample solution was subsequently investigated using double fluorescence modulations. For a complete periodic photoswitching cycle, four sequential UV pulses (365 nm) and four sequential visible light pulses (570 nm) were employed. In the first half of the period ($0 \rightarrow \pi$), the as-prepared sample was irradiated using 365-nm light for 2 s, which was followed by an immediate fluorescence spectrum acquisition using 420-nm excitation. During the first half of the period, spiropyran was converted to merocyanine. This step containing both UV irradiation and the subsequent spectrum acquisition was repeated for three more times. In the second half of the period ($\pi \rightarrow 2\pi$), 570-nm light pulses with 10-s duration were employed to irradiate the sample. During the second half period, ring-closure converted merocyanine back to spiropyran. Likewise, four 570-nm irradiation pulses were used to complete the second period. Together, four UV and four visible light pulses completed the full cycle ($0 \rightarrow 2\pi$).

Although merocyanine undergoes thermal reversion and returns to spiropyran at room temperature, such thermal reversion rate at room temperature is pretty slow as compared to the light stimulated processes. Taking this into consideration, fluorescence spectrum acquisition only scanned a narrower range (440−560 nm) using a faster integration time (0.1 s).

The acquired 420-nm excited emission spectra contained the superposition of both HMGA1-GFP signal (analyte) and the fluorescein (noise) subjected to 365- or 570-nm photoswitching modulation. The crude data contained frequency encoded signal and DC noise. Therefore, the "real" spectrum of HMGA1-GFP can be extracted by subtracting the spectra acquired when the fluorescence of HMGA1-GFP was down modulated (new "baseline") from those acquired when HMGA1-GFP was up-modulated (signal plus baseline). Specifically, four emission spectra acquired after 365-nm irradiation were mathematically cumulated, which was subsequently subtracted from the superposition of another four emission spectra acquired after 570-nm irradiation. The fluorescence intensity difference was plotted against wavelength, resulting

in the extracted fluorescence spectrum of HMGA1-GFP. After several complete modulation cycles, the background noise from fluorescein was intelligently removed and the "unpolluted" signal of the HMGA1-GFP was finally revealed (Figure 5).

Measuring the Dissociation Constants of the Donor–Acceptor Pairs. The negatively charged nanoparticle surface interacting with positively charged analytes (e.g., GFP-HMGA1) drives the dynamic equilibrium, establishing the green-emitting donor and the red-fluorescing acceptor (SP nanoparticles) pairs. Of great importance is that photoswitching can modulate both fluorescence signals. The dissociation constant for each donor–acceptor pair can be determined from the concentration quotient at the equilibrium; therefore, the concentrations to be determined are the free donor, free acceptor, and the bound donor–acceptor pair. For calculation simplification, interaction between GFP-HMGA1 and SP nanoparticle is treated as that GFP-HMGA1 molecules interact with individual carboxylic groups. Acid–base titration of the 61-nm polymer nanoparticle sample provided the "concentration" of the carboxylic groups. Dividing the total number of carboxylic groups by that of nanoparticles yielded, on average, 10 carboxylic groups per particle. Finally, the dissociation constant, K_d, is written as a quotient of the equilibrium concentrations, denoted by $[\text{GFP-HMGA1}]_{eq}$, $[\text{COO}^-]_{eq}$, and $[\text{GFP-HMGA1-COO}^-]_{eq}$:

$$\text{GFP-HMGA1} + \text{COO}^- \underset{K_d}{\overset{K_a}{\rightleftharpoons}} \text{GFP-HMGA1} - \text{COO}^- \quad (2)$$

$$K_d = \frac{[\text{GFP-HMGA1}]_{eq} \times [\text{COO}^-]_{eq}}{[\text{GFP-HMGA1-COO}^-]_{eq}} = \frac{([\text{GFP-HMGA1}]_0 - [\text{GFP-HMGA1-COO}^-]_{eq})([\text{COO}^-]_0 - [\text{GFP-HMGA1-COO}^-]_{eq})}{[\text{GFP-HMGA1-COO}^-]_{eq}} \quad (3)$$

where $[\text{GFP-HMGA1}]_0$ and $[\text{COO}^-]_0$ denote the initial concentrations of GFP-HMGA1 and carboxylic group. As a result, determining the equilibrium concentration of the bound donor–acceptor pair, $[\text{GFP-HMGA1-COO}^-]_{eq}$, will allow calculation of the dissociation constant K_d.

In a typical protocol, we used a 100-kDa cutoff filter (Millipore Amicon Ultra4 Centrifugal Filter Units) to separate the proteins from nanoparticles. The centrifugation was carried out using a 35° fixed angle rotor at 5000*g* for 15 min. The GFP-HMGA1, GFP, and fluorescein-HMGA1 proteins were estimated to be 42, 28, and 16 kDa, respectively; thus, they should freely pass the micropores filter. The proteins bound to the 61-nm nanoparticles and "free" carboxylate on the nanoparticles were filtered off. Only free proteins could pass the filter and their concentrations were determined. For instance, GFP-HMGA1 concentration was determined by measuring the fluorescence intensity at 508 nm. Although three proteins used in our experiment were smaller than 100 kDa, the 100-kDa centrifugal filters still physically adsorbed certain amount of these free proteins. These physically adsorbed proteins were accounted as the free proteins. To determine the amount of protein adsorbed by the filter physically, we let pure protein samples, for instance GFP-HMGA1, pass through the centrifugation filter under identical experimental conditions in the absence of polymer nanoparticles. The loss of protein (e.g., GFP-HMGA1) denoted as $[\text{GFP-HMGA1}]_{bl}$ was added to the calculation. Thus, the immediately measured "free" protein (e.g., GFP-HMGA1) that passed through the centrifugal filter in the presence of polymer nanoparticles is actually an "apparent" equilibrium concentration, denoted as $[\text{GFP-HMGA1}]_{ap}$. The real equilibrium concentration of the protein (e.g., GFP-HMGA1) in the equilibrium prior to centrifugation treatment, denoted as $[\text{GFP-HMGA1}]_{eq}$, should be the sum of $[\text{GFP-HMGA1}]_{bl}$ and $[\text{GFP-HMGA1}]_{ap}$. Once $[\text{GFP-HMGA1}]_{eq}$ was known, $[\text{GFP-HMGA1-COO}^-]_{eq}$ and the "free" carboxylate concentration $[\text{COO}^-]_{eq}$ could be easily calculated using eqs 4 and 5, respectively:

$$[\text{GFP-HMGA1-COO}^-]_{eq} = [\text{GFP-HMGA1}]_0 - [\text{GFP-HMGA1}]_{eq} \quad (4)$$

$$[\text{COO}^-]_{eq} = [\text{COO}^-]_0 - [\text{GFP-HMGA1-COO}^-]_{eq} \quad (5)$$

Applying the obtained equilibrium concentrations to eq 3, the dissociation constant for eq 2 was obtained.

AUTHOR INFORMATION

Corresponding Author
zytian@gucas.ac.cn; dequan@wsu.edu

ACKNOWLEDGMENT

Z. Y. Tian thanks the support from the "CAS Hundred Talent Program" starting grant of GUCAS and we thank the support from the National Science Foundation (CHE-0805547).

REFERENCES

(1) Chan, W. C. W.; Maxwell, D. J.; Gao, X. H.; Bailey, R. E.; Han, M. Y.; Nie, S. M. *Curr. Opin. Biotechnol.* **2002**, *13*, 40.
(2) Ballou, B.; Ernst, L. A.; Waggoner, A. S. *Curr. Med. Chem.* **2005**, *12*, 795.
(3) Medintz, I. L.; Uyeda, H. T.; Goldman, E. R.; Mattoussi, H. *Nat. Mater.* **2005**, *4*, 435.
(4) Santra, S.; Dutta, D.; Walter, G. A.; Moudgil, B. M. *Technol. Cancer Res. Treat.* **2005**, *4*, 593.
(5) Toprak, E.; Selvin, P. R. *Annu. Rev. Biophys. Biomol. Struct.* **2007**, *36*, 349.
(6) Aubin, J. E. *J. Histochem. Cytochem.* **1979**, *27*, 36.
(7) Monici, M. *Biotechnol. Annu. Rev.* **2005**, *11*, 227.
(8) Wu, W. W.; Li, A. D. Q. *Nanomedicine* **2007**, *2*, 523.
(9) Rocker, C.; Potzl, M.; Zhang, F.; Parak, W. J.; Nienhaus, G.; U. *Nat. Nanotechnol.* **2009**, *4*, 577.
(10) De, M.; Rana, S.; Akpinar, H.; Miranda, O. R.; Arvizo, R. R.; Bunz, U. H. F.; Rotello, V. M. *Nat. Chem.* **2009**, *1*, 461.
(11) Cedervall, T.; Lynch, I.; Foy, M.; Berggad, T.; Donnelly, S. C.; Cagney, G.; Linse, S.; Dawson, K. A. *Angew. Chem., Int. Ed.* **2007**, *46*, 5754.
(12) Cedervall, T.; Lynch, I.; Lindman, S.; Berggad, T.; Thulin, E.; Nilsson, H.; Dawson, K. A.; Linse, S. *Proc. Natl. Acad. Sci. U.S.A.* **2007**, *104*, 2050.
(13) Lundqvist, M.; Stigler, J.; Elia, G.; Lynch, I.; Cedervall, T.; Dawson, K. A. *Proc. Natl. Acad. Sci. U.S.A.* **2008**, *105*, 14265.
(14) Truong, K.; Sawano, A.; Mizuno, H.; Hama, H.; Tong, K. I.; Mal, T. K.; Miyawaki, A.; Ikura, M. *Nat. Struct. Biol.* **2001**, *8*, 1069.
(15) Li, I. T.; Pham, E.; Truong, K. *Biotechnol. Lett.* **2006**, *28*, 1971.
(16) Periasamy, A. *J. Biomed. Opt.* **2001**, *6*, 287.
(17) Jares-Erijman, E. A.; Jovin, T. M. *Nat. Biotechnol.* **2003**, *21*, 1387.
(18) Gumbleton, M.; Stephens, D. J. *Adv. Drug Delivery Rev.* **2005**, *57*, 5.
(19) Sanden, T.; Persson, G.; Thyberg, P.; Blom, H.; Widengren, J. *Anal. Chem.* **2007**, *79*, 3330.
(20) De, A. K.; Goswami, D. *J. Fluoresc.* **2009**, *19*, 381.
(21) Fernandez-Suarez, M.; Ting, A. Y. *Nat. Rev. Mol. Cell Biol.* **2008**, *9*, 929.
(22) Heilemann, M.; Dedecker, P.; Hofkens, J.; Sauer, M *Laser Photonics Rev.* **2009**, *3*, 180.
(23) Tian, Z. Y.; Wu, W. W.; Li, A. D. Q. *ChemPhysChem* **2009**, *10*, 2577.
(24) Tian, Z. Y.; Wu., W. W.; Li, A. D. Q. Photoswitchable Nanoprobes for Biological Imaging Applications. In *Trace Analysis with*

Nanomaterials; Pierce, D. T., Zhao, J. X., Eds.; Wiley-VCH: Weinheim, 2010; pp3−30.
(25) Betzig, E.; Patterson, G. H.; Sougrat, R.; Lindwasser, O. W.; Olenych, S.; Bonifacino, J. S.; Davidson, M. W.; Lippincott-Schwartz, J. *Science* **2006**, *313*, 1642.
(26) Rust, M. J.; Bates, M.; Zhuang, X. W. *Nat. Methods* **2006**, *3*, 793.
(27) Hess, S. T.; Girirajan, T. P. K.; Mason, M. D. *Biophys. J.* **2006**, *91*, 4258.
(28) Egner, A.; Geisler, C.; Von Middendorf, C.; Bock, H.; Wenzel, D.; Medda, R.; Andresen, M.; Stiel, A. C.; Jakobs, S.; Eggeling, C.; Schonle, A.; Hell, S. W. *Biophys. J.* **2007**, *93*, 3285.
(29) Bates, M.; Huang, B.; Dempsey, G. T.; Zhuang, X. W. *Science* **2007**, *317*, 1749.
(30) Hu, D. H.; Tian, Z. Y.; Wu, W. W.; Wan, W.; Li, A. D. Q. *J. Am. Chem. Soc.* **2008**, *130*, 15279.
(31) Tian, Z. Y.; Wu, W. W.; Wan, W.; Li, A. D. Q. *J. Am. Chem. Soc.* **2009**, *131*, 4245.
(32) Zhu, L. Y.; Wu, W. W.; Zhu, M. Q.; Han, J. J.; Hurst, J. K.; Li, A. D. Q. *J. Am. Chem. Soc.* **2007**, *129*, 3524.
(33) Gorner, H. *Chem. Phys.* **1997**, *222*, 315.
(34) Gorner, H. *Chem. Phys. Lett.* **1998**, *282*, 381.
(35) Bohne, C.; Fan, M. G.; Li, Z. H.; Laing, Y. C.; Lusztyk, J.; Scaiano, J. C. *J. Photochem. Photobiol., A* **1992**, *66*, 79.
(36) Wojtyk, J. T. C.; Wasey, A.; Kazmaier, P. M.; Hoz, S.; Buncel, E. *J. Phys. Chem. A* **2000**, *104*, 9046.
(37) Richards, C. I.; Hsiang, J. C.; Senapati, D.; Patel, S.; Yu, J. H.; Vosch, T.; Dickson, R. M. *J. Am. Chem. Soc.* **2009**, *131*, 4619.
(38) Li, A. D. Q. *NSF Proposal* **2006**, 0715439.
(39) Mao, S.; Benninger, R. K. P.; Yan, Y. L.; Petchprayoon, C.; Jackson, D.; Easley, C. J.; Piston, D. W.; Marriott, G. *Biophys. J.* **2008**, *94*, 4515.
(40) Marriott, G.; Mao, S.; Sakata, T.; Ran, J.; Jackson, D. K.; Petchprayoon, C.; Gomez, T. J.; Warp, E.; Tulyathan, O.; Aaron, H. L.; Isacoff, E. Y.; Yan, Y. L. *Proc. Natl. Acad. Sci. U.S.A.* **2008**, *105*, 17789.
(41) Li, A. D. Q.; Zhan, C. L.; Hu, D. H.; Wan, W.; Yao, J. N. *J. Am. Chem. Soc.* **2011**, *133*, 7628.
(42) Peng, X. Z.; Chen, H. X.; Draney, D. R.; Volcheck, W.; Schutz-Geschwender, A.; Olive, D. M. *Anal. Biochem.* **2009**, *388*, 220.
(43) Sanchez-Martinez, M. L.; Aguilar-Caballos, M. P.; Gomez-Hens, A. *Anal. Chem.* **2007**, *79*, 7424.
(44) Harma, H.; Sarrail, G.; Kirjavainen, J.; Martikkala, E.; Hemmila, I.; Hanninen, P. *Anal. Chem.* **2010**, *82*, 892.